AEROPHYSICAL STUDIES AT HYPERSONIC VELOCITIES IN FREE FLIGHT RANGES

By C. J. MAIDEN

Section Leader, Hypersonic Physics Section
Canadian Armament Research and Development Establishment

1.0 INTRODUCTION

THE advantages of using a free-flight range in order to study aerophysical phenomena associated with very high speed flight have been discussed by Bull[1]. One advantage in particular is that the free-flight range offers a relatively inexpensive technique for studying re-entry phenomena under controlled laboratory conditions. That controlled conditions are required for such a study is obvious when one considers the complex nature of the phenomena associated with flight at hypersonic velocities. For instance, any optical or radar observations on a hypersonic body are dependent upon the physico-chemical processes occurring in the near flow field and in the wake of the body. In turn these processes are dependent upon body shape, size, composition, orientation, altitude and velocity.

The Canadian Armament Research and Development Establishment has four operational free-flight ranges in which models up to several inches piameter can be observed when travelling at high velocities. Current research in these facilities includes stability studies and investigations of the plasma generated by a hypervelocity body. The present paper describes the results of optical and radar observations on $\frac{1}{2}$. in. diameter models travelling at hypersonic velocities in the CARDE Range 1 facility. The measurements presented have been obtained in the past year, during which time three successive hypersonic physics programmes have been completed. The results of each of these programmes has determined, to a large extent, the instrumentation and test requirements for the following programme. Hence, for continuity requirements, the experimental results are presented in three sections, each section corresponding to a test programme. It will be noted that during the course of these programmes considerable advances were made in velocity capability of the light gas guns used to launch the models.

2.0 DESCRIPTION OF FACILITY

Full details of the CARDE Range 1 facility are presented in reference 2, hence, only a brief description of the facility will be given here. The Range is shown diagrammatically in Fig. 1 and is seen to consist essentially of a 50 ft long tank evacuated to simulate altitude. A dump tank,

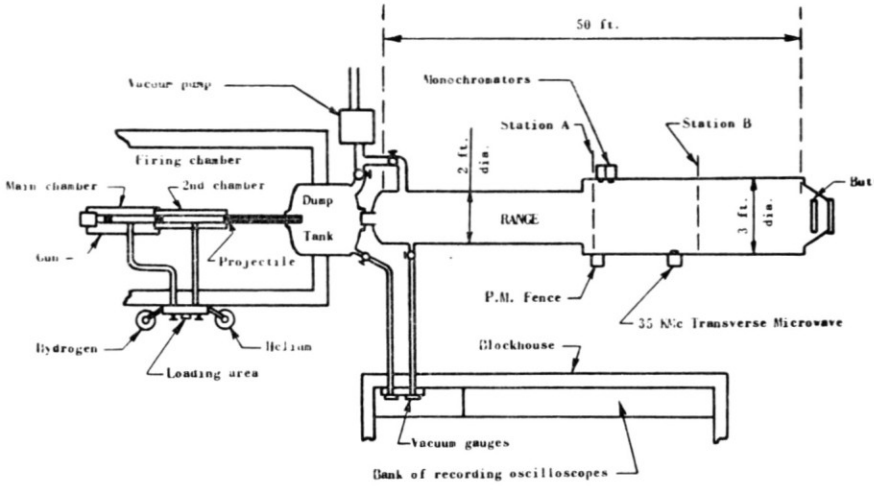

FIG. 1. Diagrammatic representation of the Range Facility.

with flap valve, is provided to trap the gun gases and to permit the evacuation of the gun barrel independently of the range. The highest vacuum obtained to date on the range corresponds to an altitude of 225,000 ft (100 microns of Hg pressure). To measure the projectile velocity interruption type light screens are used in conjunction with shadowgraph photographic stations. Three such stations are at present in use.

A three-stage light gas gun was used to launch one half-inch diameter models of various shapes and materials into the range at hypersonic velocities. The present peak capability of the gun is 22,000 ft/sec, however, it is felt that this can be extended to near 30,000 ft/sec. The principle of the three stage light gas gun is given in references 2 and 3.

3.0 EXPERIMENTAL RESULTS

3.1 *The First Programme*

The spectroscopic character of the luminosity created by high velocity pellets of several metallic materials in atmospheric air was first investigated by Rinehart, Allen and White[4]. The pronounced features of the spectra

obtained were atomic lines and oxide bands of the pellet material. This work at atmospheric pressure was extended by Allen and Mayfield[5] who obtained time resolved spectra. They concluded that most of the luminosity was produced from the oxidation of material ablated from the pellet. The purpose of the first programme on CARDE Range 1 was to obtain further preliminary measurements of the luminosity generated by a hypersonic body. Information was sought concerning the geometrical distribution of the luminosity surrounding a projectile, the peak luminosity produced at various velocities and pressures, and the contribution of ablation products to the light emitted.

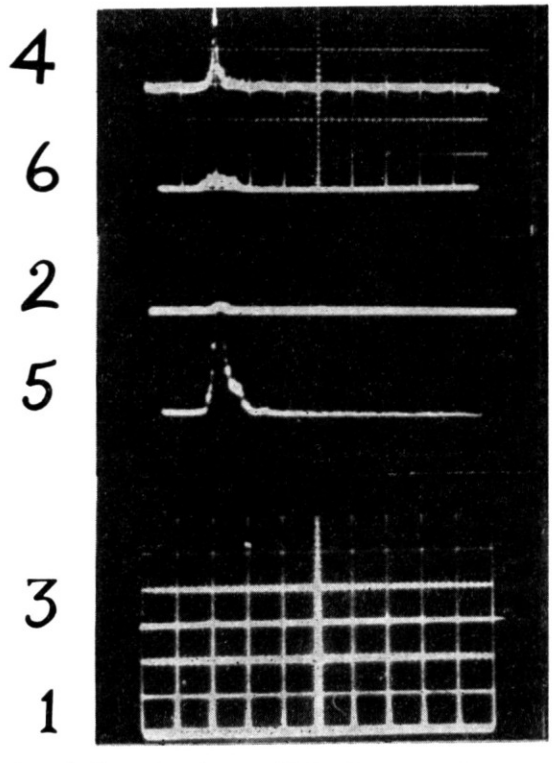

FIG. 2. Typical result from the photomultiplier fence. Velocity: 11400 ft/sec. Pressure: 50 mm. Sweep speed: 20 μsec/div.

In the programme 130 cylindrical aluminium pellets, 0.4 in. in length, were launched at velocities from 7000 to 14,000 ft/sec in range pressures of 5 mm (116,000 ft) to 200 mm (38,000 ft) of mercury. Initial attempts to obtain time integrated spectra at the above pressures proved fruitless due to the low light intensities involved, hence, it was decided to use photoelectric techniques for all luminosity measurements. The first apparatus

constructed was a photomultiplier fence. The unit consisted of six 1P21 photomultipliers, sensitive in the wavelength region 3400Å to 5400Å, with each photomultiplier having a 3/16 in. × $1\frac{1}{4}$ in. field of view at the centre of the range. Thus the total field of view was a vertical slit 3/16 in. wide by $7\frac{1}{2}$ in. high. A typical result obtained from the unit is shown in Fig. 2 with the channels identified from top to bottom of the field of view. In this test the projectile velocity was 11,500 ft/sec, the range pressure 5 mm and the projectile passed between channels 4 and 5. Several conclusions were drawn from results obtained with this unit.

Firstly, conclusions were obtained regarding where the luminous signal started with respect to the projectile. This was done by comparing the delay time, between the trigger pulse from the photographic station and the output pulse from the photomultipliers, with the calculated flight time between the photographic station and the fence. Considering all the successful shots in the programme the average difference in these two times was 6μsec. This small difference indicates that the peak radiation was located somewhere within the length of the projectile, almost certainly from the stagnation region. It is considered that any discrepancy in the two times can be attributed to the light screen triggering late, and in some cases to imperfect triggering of the oscilloscopes. It is interesting to note that Davidson and Partridge[6] found, from observations on aluminium pellets in atmospheric air, that there was a delay between the time when the pellet passed a given point and when the light passed the same point. These investigators suggested that the main pulse of luminosity was produced by energy released from the oxidation of aluminium droplets ablated from the body. No such delay time before the emission of light was observed in the present tests.

The second study concerned the geometrical distribution of luminosity surrounding a projectile. On many shots the sharp pulse observed on channels 4 and 5 in Fig. 2 was seen on one channel only. From the geometrical details of the system it can thus be concluded that this very intense region was less than $1\frac{1}{4}$ in. wide. This is reasonable, as the majority of the gaseous radiation generated by a hypersonic cylindrical projectile is expected to come from a stagnation region of diameter approximately equal to the cylinder diameter. Also, any luminosity in the near flow field of the body due to ablation products should be confined to the boundary layer. In most tests the sharp pulse of luminosity was only a few microseconds wide at half maximum points and little wake luminosity could be seen. However, in the tests where the peak signal was permitted to go off the oscilloscope screen, some wake characteristics were observed. Generally the trails decayed exponentially, however, at the higher pressures some prior fluctuations were evident for a few inches behind the

projectile. These fluctuations could possibly be caused by the reverse flow field and recompression shocks just behind the projectile.

The photomultiplier fence was calibrated using a tungsten lamp. From this calibration the value of the peak luminosity emitted in each of the tests was determined by assuming a constant detector responsivity between 3400Å and 5400Å. A large scatter (factor of 10 or more) was observed between the results of seemingly identical tests. This scatter can be attributed to several factors, perhaps the most important of which is pellet instability. The projectile orientation when opposite the fence, and hence the volume of stagnation gas producing most of the light, varied considerably from test to test. Other factors that could cause variations under identical test conditions are atmospheric impurities, variations in distance between the projectile and fence, and a symmetrical ablation from the projectile. However, despite the scatter in the results obtained there was definite tendency for the luminosity to increase with increasing velocity and range pressure. The limits of measured peak intensities at the five test pressures are presented in Table 1.

TABLE 1

Peak Luminous Intensities From Cylindrical Aluminium Projectiles

Pressure mm	Velocity range ft/sec.	Range of peak intensities ergs sec^{-1} $ster^{-1}$
200	8000–14000	1.6×10^{5}–10^{8}
100	9000–13000	2×10^{4}–2.4×10^{1}
50	8000–14000	2×10^{4}–1.8×10^{6}
25	8000–14000	1.2×10^{4}–6×10^{4}
10	8000–14000	1.4×10^{4}–4×10^{4}

In addition to the photomultiplier fence, two monochromators were used with the intention of investigating the contribution of ablation products to the luminosity generated by a hypersonic projectile. The first monochromator was a Perkin Elmer instrument in which radiation covering a desired spectral range could be focussed on a 1P21 photomultiplier. The spectral region chosen for the tests was the 100A° interval from 4792Å to 4892Å. This wavelength band was chosen as it includes three strong aluminium oxide bands (4842Å, 4866Å and 4888Å) observed in previous spectroscopic studies (4,5) on the light emitted by high speed aluminium pellets. The field of view of this unit at the centre of the range was $4\frac{1}{2}$ in. high and the width was varied from 0.27 to 0.46 in. The signals obtained during the tests were similar to that shown in Fig. 3(a) and differ little in shape from the signals observed with the fence. Also, the luminosity

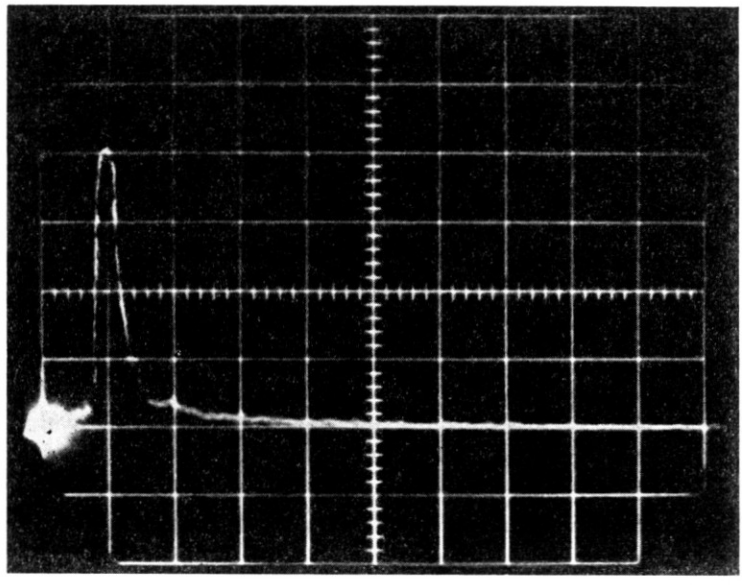

a

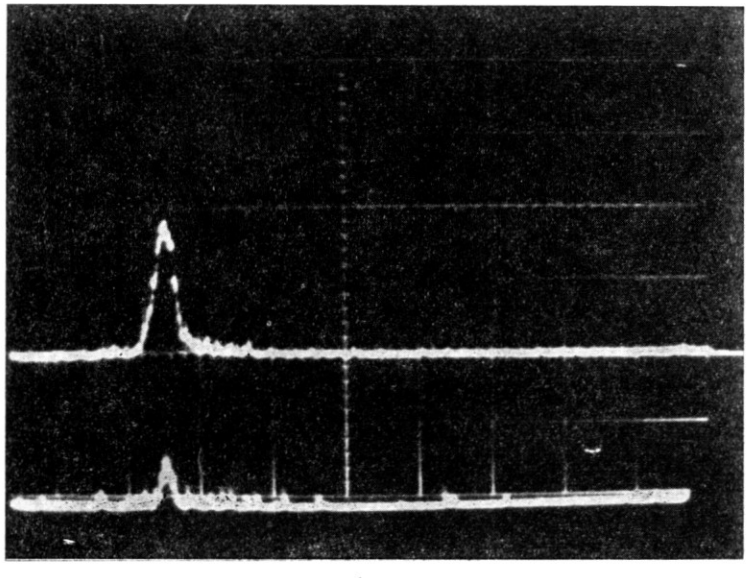

b

FIG. 3. Monochromator results.
(a) Single channel. Velocity: 11600 ft/sec. Pressure: 50 mm.
Sweep speed: 20 μsec/div.
(b) Double channel. Velocity: 12600 ft/sec. Pressure: 100 mm.
Sweep speed: 10 μsec/div. Upper trace centered at 48424Å.
Lower trace centered at 3950Å.

was found to originate when the projectile appeared in the field of view. Hence, the logical conclusion is that the light emitted in the wavelength band from 4792 to 4892Å originated from the same region of the flow field as the light emitted in the interval 3400Å to 5400Å. The monochromator was not calibrated for absolute radiation measurements, however, two remarks regarding intensity can be made. Firstly, there was a definite trend for an increase in radiation level with increasing velocity and pressure; and secondly, for identical test conditions, there was a large scatter in peak radiant emission.

The other monochromator was a double channel monochromator constructed from a Hilger glass prism spectograph in which the dispersed light was blanked off so as to permit the light from two 20Å bands to be viewed separately by 1P21 photomultipliers. From the work of Rhinehart, Allen and White[4] it was decided to view the 20Å regions centered at 4842Å and 3952Å. Thus the first 20Å covered the A10 band at 4842Å and the second 20Å band covered the two A1 lines at 3944Å and 3961Å. A typical result from this unit is shown in Fig. 3(b). It is seen that the signals are very similar in shape to those obtained with the photomultiplier fence and single channel monochromator. This indicates that, for the present test conditions, a high continuum in the two 20Å bands could be masking any A10 band or A1 line emission, and suggests that luminosity due to ablation effects is not predominant over gaseous radiation. The other results obtained with the double channel monochromator are consistent with this tentative conclusion.

Thus the results of the first programme, while giving rough estimates of peak luminosity and geometrical distribution of luminosity, do not permit any definite conclusions concerning the contribution of ablation products to the visible light produced by a high speed pellet. Also, the shape and instability of the projectiles makes the comparison of the results with theory almost impossible. The second programme was planned with these points in mind.

3.2 *The Second Programme*

The apparatus used in the second programme consisted of two single photomultiplier units, sensitive in the same wavelength region as the fence (3400–5400Å). Each of these units consisted essentially of two slits in front of a 1P21 photomultiplier so that the field of view at the centre of the range was a vertical slit of dimensions $7\frac{1}{2} \times \frac{1}{8}$ in. The two units were placed at positions 10 ft. apart on the range. These positions were termed Station A and Station B respectively. During this programme 0.4 in. diameter spheres of aluminium, magnesium and ethocel plastic were launched at velocities from 10,000 to 15,000 ft/sec. at a range pres-

sure of 1.65 mm (140,000 ft). The spheres were sabot launched and the sabot was permitted to follow the sphere down the range. A typical result is presented in Fig. 4 and the signals from the sphere and sabot are clearly observed. From the calibration of the units the value of the peak radiation

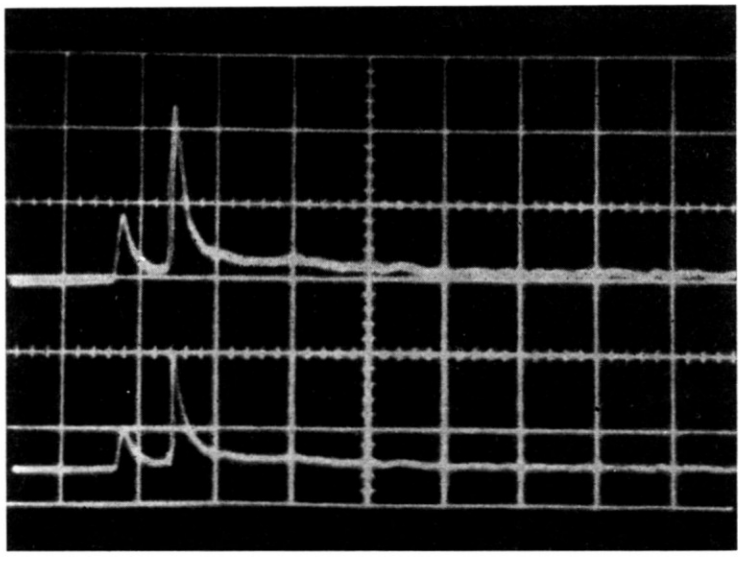

FIG. 4. Typical result from a 1P21 photomultiplier unit. Velocity: 12000 ft/sec. Pressure: 1.65 mm. Sweep speed: 20 μsecs/div. Gain: Upper beam 0.1 V/div. lower beam 0.2 V/div. Signal on the left is from the aluminium sphere.

emitted in each of the tests was determined by assuming a constant photomultiplier responsivity between 3400Å and 5400Å. The results are presented in Fig. 5 and it is seen that, although there is a significant scatter in the results, there is no definite trend for one material to give a greater luminous output than another material. This indicates that the contribution of ablation products to the nose cap luminosity at 1.65 mm is small. Also, there was no tendency for the furthest downrange unit to record a consistently higher output that the first unit. Before comparing the results presented in Fig. 5 with theoretical predictions, a few remarks are relevant concerning the phenomena that can occur behind the bow shock of a hypersonic body.

A body travelling at hypersonic velocity excites the air to sufficiently high temperatures for real gas effects to be important in the flow field around the body. When the bow shock wave of a high speed projectile impinges upon the air some of the shock's translational motion is converted into other energy modes such as random translation, rotation, vibration, dissociation and ionisation. The temperature at any point

behind the shock is governed by the energy of random translation. Hence, as finite times are required to convert random translational energy to other energy modes, the temperature behind the shock falls before full

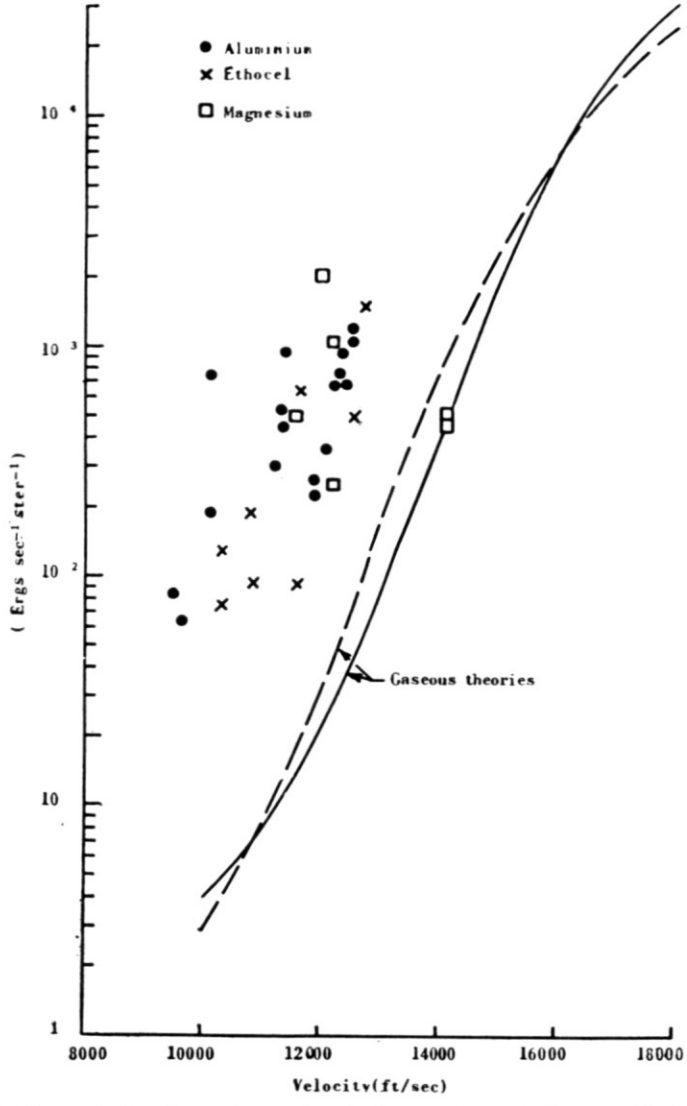

FIG. 5. Theoretical and experimental radiation results at 1.65 mm $\pm$ 0.25 mm.

thermodynamic equilibrium is attained. A good review of relaxation phenomena occurring in shock fronts has been presented by Shkarosky *et al.*[7]. In the present paper, full thermodynamic equilibrium conditions are assumed in order to calculate the theoretical nose cap radiation. The

flight conditions at which non-equilibrium effects become important are then estimated.

For a range of velocities and altitudes the equilibrium temperature and density at the stagnation point of a hypersonic body has been tabulated by Feldman[8]. From these values the corresponding stagnation point particle concentrations can be determined from Gilmore's tables[9]. For the present paper, it was necessary to extend this work and determine equilibrium gaseous properties at all points in the nose cap of a hypersonic sphere. The method chosen to do this was developed by Maslen

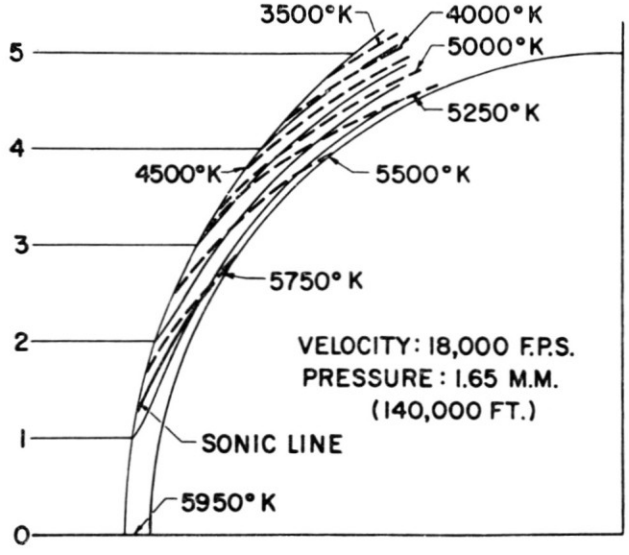

FIG. 6. Theoretical nose cap solution for a sphere.

and Moeckel[10], and is one of a number of available techniques[11]. In this method inviscid flow is considered and equilibrium gas conditions are assumed at every point in the flow field. The initial conditions are a known shock detachment distance[12], a known pressure distribution on the body surface (Newtonian) and an assumed shock shape. The method is certainly not the best available, particularly because prior knowledge is required of the pressure distribution on the body. However, for the immediate purpose of calculating the radiation emitted from the stagnation region of a sphere, the method is considered adequate. Solutions were obtained for velocities of 10,000, 12,000, 14,000 and 18,000 ft/sec at a pressure of 1.65 mm. Figure 6 shows the calculated shock shape, streamline pattern, temperature contours and sonic line for a velocity of 18,000 ft/sec. The radiation emitted between 3400 and 5400Å by the nose cap of a 0.4 in. sphere was calculated from the flow field properties in the following

manner. Keck *et al.*[13] have shown that the visible emissivity of air in equilibrium can be represented by

$$\varepsilon = 7.65 \times 10^{-2}\left(\frac{T}{8000}\right)^{6} \times \frac{\varrho}{\varrho_0} \tag{1}$$

where ε is the emissivity per cm thickness of gas, T and ϱ are the temperature and density of the air, and ϱ_0 is sea level density. Thus the intensity of radiation emitted (cm^3) ster. from air at temperature T and density ϱ between 3400 and 5400Å is given by

$$I = \frac{\varepsilon}{\pi} \int_{3400}^{5400} J_\lambda \, d_\lambda \tag{2}$$

where J_λ is the intensity of radiation per unit wavelength from a black body at temperature T[14]. Hence, to calculate the radiation from a flow field as in Fig. 6, the shock cap was partitioned into several hundred volume elements, each of assumed constant temperature and density. The sum of the contribution from each element, as calculated from Eq. 2, gave the total radiant output. The final results are presented in Figure 5. It is interesting to compare these theoretical intensities with approximate values calculated by a method due to Feldman[15]. In this method the total radiation is calculated by multiplying the stagnation point radiation per unit volume by an effective volume of 0.1 r^3, where r is the nose radius of the body. According to Feldman this effective volume should give the correct amount of total radiation from a nose cap. To check this hypothesis the value of I in Eq. 2 has been calculated for various velocities and altitudes using stagnation values of temperature and density (8). The resulting contours of constant emitted radiation per unit volume are presented in Fig. 7. Hence, to obtain the radiation emitted from the nose cap of a sphere of radius r in the wavelength band 3400Å to 5400Å, the relevant value of I has only to be multiplied by 0.1 r^3. The theoretical radiation curve, for a 0.4 in. sphere at 1.65 mm has been calculated in such a manner and is shown dashed in Fig. 5. It is seen that the agreement with the more exact solution is very good.

The theoretical curves in Figs. 5 and 7 have been calculated assuming the nose cap to be in full thermodynamic equilibrium. As mentioned previously there is a non-equilibrium region associated with the formation of a shock in which temperatures are greater than the final equilibrium temperature. The shock tube has been used to investigate this non-equilibrium region[16, 17]. From the results of this research Feldman[15] has presented, on a velocity altitude chart, contours of the distance d behind a normal shock necessary for the temperature to relax to 35% above its equilibrium value. If it is assumed that non-equilibrium effects will become

important when the relaxation distance d equals the shock detachment distance[12], then Fig. 7 can be separated into equilibrium and non-equilibrium regions. The delineating curve for a 0.4 in. sphere is shown dashed in Fig. 7 and can be scaled to other sphere diameters by use of the experimental relationship that $r\rho/\rho_0$ is constant at a constant velocity[16].

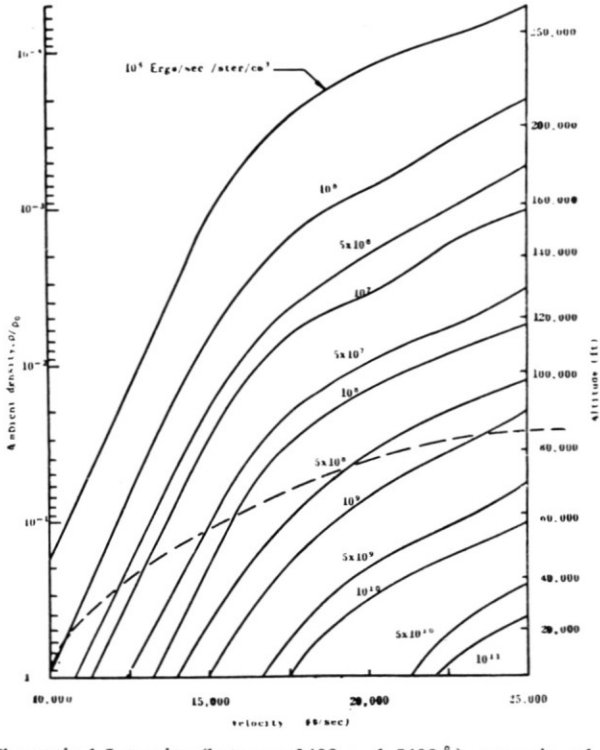

FIG. 7. Theoretical Intensity (between 3400 and 5400Å) per unit volume from stagnation point gas.

In the non-equilibrium region the gaseous radiation is expected to be greater than indicated from equilibrium considerations because of the high non-equilibrium temperatures at the nose cap. Figure 5 shows that certainly at 1.65 mm, which is well into the non-equilibrium region for a 0.4 in. sphere, the experimentally measured radiation is significantly greater than equilibrium estimates.

Thus the second programme has indicated that at 1.65 mm ablation effects are small and the experimentally measured peak luminosity is in reasonable agreement with theory. The third experimental programme had two purposes. The first of these was to extend the nose cap measurements, and the second was to make optical and microwave observations on the wake of a hypersonic projectile.

3.3 *The Third Programme*

3.3.1 *Nose cap studies*—For this programme, additional single photomultiplier units were mounted on the range at stations A and B. The photomultipliers at station A consisted of one 1P21, one RCA 6217 and two RCA 1P28 units with wide and narrow band filters respectively. The

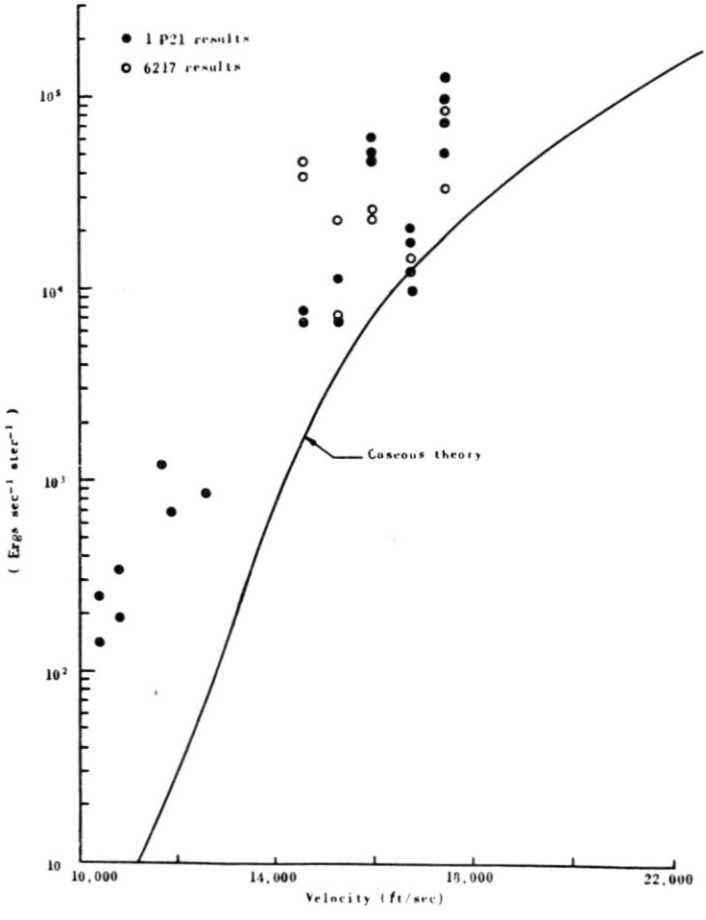

FIG. 8(a). Theoretical and experimental radiation results. at 1.65 mm $\pm$ 0.25 mm.

instrumentation at station B was identical to that at station A, except for the addition of two more 1P21 units mounted so that the three 1P21 photomultipliers were at 120° to each other on the circumference of the range. The effective wavelength bands of these units, between half maximum sensitivity points, are 3400–5400Å for the 1P21 detectors, 3500–6000Å for the 6217 units, 2450–3850Å for the 1P28 detectors

with wide band filters and 2450 to 3000Å for the latter detectors with narrow band filters.

The programme is at present unfinished; however, to date observations have been made on 0.4 in. ethocel spheres at range pressures of 1.65 mm and 76 mm. The values of peak luminosity measured by the 1P21 photo-

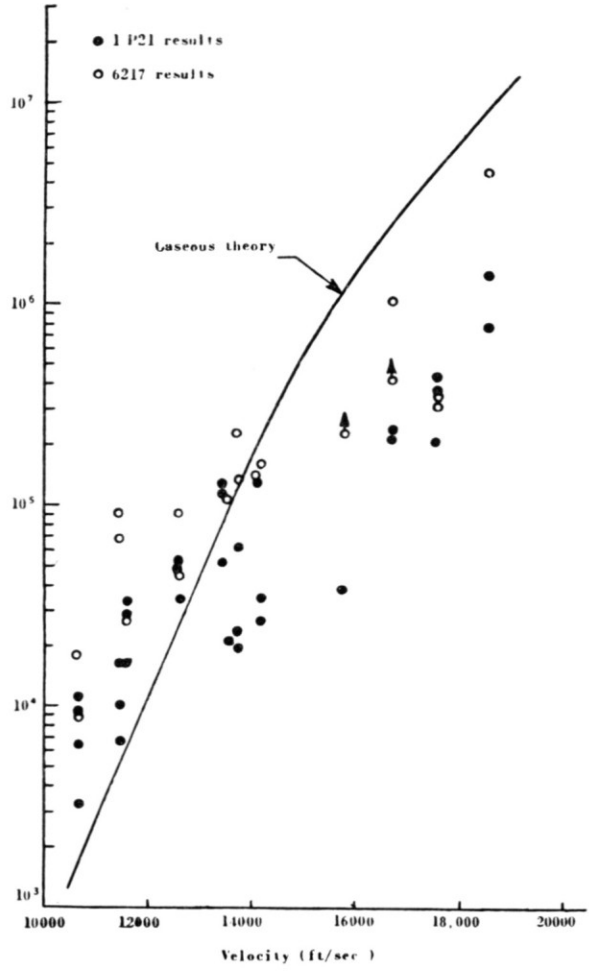

FIG. 8(b). Theoretical and experimental radiation results. at 76 mm ± 4 mm.

multipliers at these pressures are shown in Figure 8. The results presented in Fig. 8(a) are similar to the lower velocity results shown in Fig. 5 in that the experimental points lie significantly above theory. However, the experimental points at 76 mm tend to be slightly below theory at the higher velocities. Figure 7 indicates that the nose cap gas at 76 mm

should be in equilibrium, and hence one would expect the results at 76 mm to be lower with respect to theory than the results at 1.65 mm. It is interesting to observe that in Fig. 8 there is a significant scatter in the results There was no trend for a detector at station B to give a consistently greater output than a similar detector at station A; however, it was found that the outputs from the three 1P21 photomultipliers at station B were only consistent with each other to a factor of two. This is puzzling as the photomultiplier calibrations are accurate to within 10% and the fields of view are identical. It seems likely that the scatter is caused by a projectile being a few inches off axis, and hence being at a different distance from each unit. Only the 1P21 and 6217 photomultipliers have been calibrated to date. The theoretically estimated peak radiation for the sensitivity region of the 6217 detector is within 20% of the theoretical curves shown in Fig. 8; hence, the experimental points at the two test pressures have also been presented in this figure. At the moment the results from the 1P28 detectors cannot be compared with theory; however, the peak voltages varied with velocity in much the same manner as the results in Fig. 8.

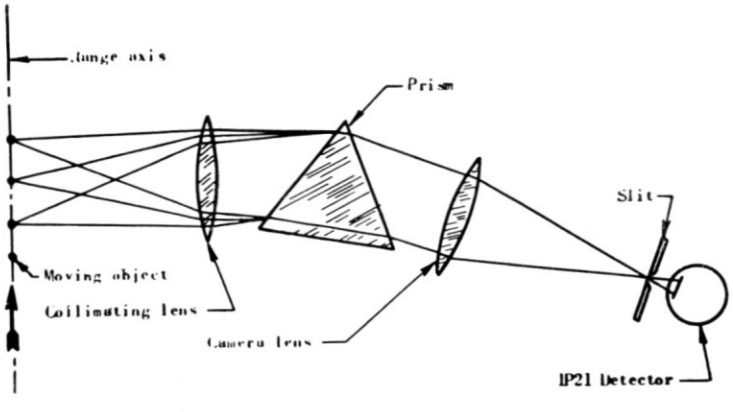

FIG. 9(a). Diagrammatic representation of moving target scan monochromator.

A moving target scan monochromator, shown diagrammatically in Fig. 9(a) was also used in the third programme. The purpose of this instrument was to observe the spectrum of the luminosity emitted from the nose cap of a hypersonic projectile. The principle of the instrument is that a point source of light, approximated by the stagnation region in the present tests, acts as an entrance slit of the monochromator, and the motion of the point source provides spectral scan in front of the exit slit. Thus the output of the photomultiplier (1P21), presented on an oscilloscope, gives a direct presentation of the absolute intensity of radiation against wavelength. Typical results from the unit are also shown in Figure

9. Figure 9(b) is a mercury spectrum obtained by reflecting the light from a mercury source on a rotating mirror, and using the reflection focussed on a ground glass as the moving point source; and Fig. 9(c) shows the

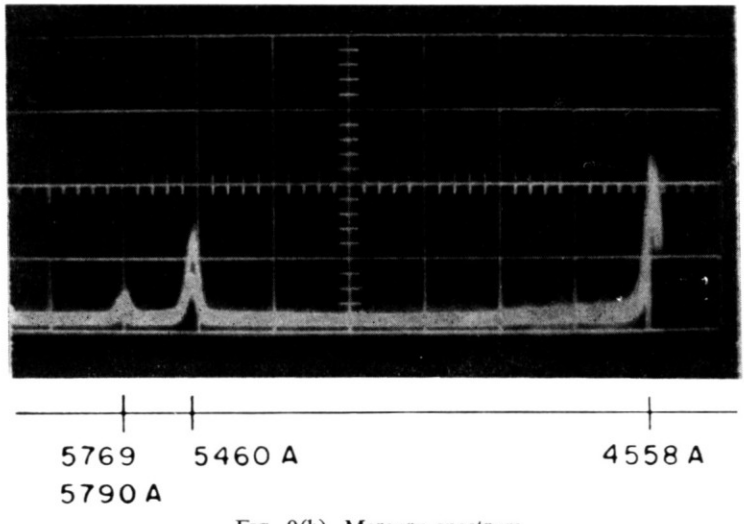

FIG. 9(b). Mercury spectrum.

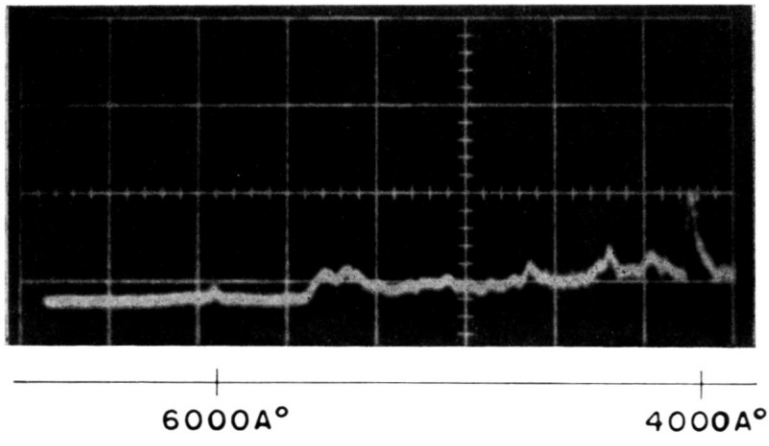

FIG. 9(c). Spectrum from ethocel sphere at 17500 ft/sec and 1·65 mm. Sweep speed: 5 μsec/div.

spectrum obtained from an ethocel sphere at 17,500 ft/sec and 1.65 mm pressure. The results so far obtained from the unit have shown the existence of a strong continuum at 1.65 mm and 76 mm, with indications that the spectral structure is more pronounced at 1.65 mm than at 76 mm. The position of the peaks at a given pressure was found to be exactly re-

peatable, but their relative amplitudes varied with velocity. At the moment, the wavelength corresponding to a given point on the trace is determined from the estimated projectile position in the field of view. This method is not very accurate and has not permitted the identification of the peaks, however, an accurate calibration, suggested by St. Pierre[18], will be available shortly. The work of Keck *et al.*[19] indicates that the observed continuum is almost certainly from No β unresolved bands, and that the masking effect of this continuum over any other band system, such as N_2^+ first negative, should be greater at 76 mm than at 1.65 mm. Also, if any of the peak are due to range contaminants (CN, C or Na), their effect on the gross luminosity measurements would be small because of the large continuum radiation. These remarks apply to the present test conditions and to the wavelength band over which the instrument is sensitive (4000–6000Å).

3.3.2 *Wake studies*—Ideally one would like to know the gas chemistry and thermodynamic properties at all points in the wake of a hypersonic body. Theoretically the problem is most complex due to the fact that these parameters are affected by body size, shape, composition, orientation, velocity, altitude and whether or not trail is laminar or turbulent. Depending upon these parameters various regions of the wake can be in chemical equilibrium, out of equilibrium or effectively chemically frozen. Also, equilibrium is attained in the front of a body by two body collisions, whereas, recombination in the wake is governed by slower three body collisions. Hence, it is possible for the flow to be in equilibrium at the nose cap but out of equilibrium in the wake. In this regard Goulard[20] has developed a criterion to determine the tendency of the flow to stay in equilibrium at any point in the flow field. The condition of full thermodynamic equilibrium in a laminar wake has received the most theoretical attention[15, 20]. Feldman[15], who is considering this case has divided the trail into two parts. Firstly, the expansion controlled wake which is the region up to a point where the pressure decays to the free stream value and cooling is controlled by the expansion of the flow; and secondly, the conduction controlled wake where the trail cools mainly by diffusion of heat away from the high temperature core. At the moment the results of such an analysis can only be compared semi-quantitatively with the radiation and microwave trail measurements made in the present tests.

Figure 10 presents traces obtained from the 1P21 and 1P28 photomultiplier units at a velocity of 11,400 ft/sec and a pressure of 76 mm. The signal on the left of each trace is from the sphere and the other signal is from the sabot. It is seen that the signal from the sphere decays rapidly from peak value, whereas, the signal from the sabot rises again after the peak and then decays in an approximately exponential manner.

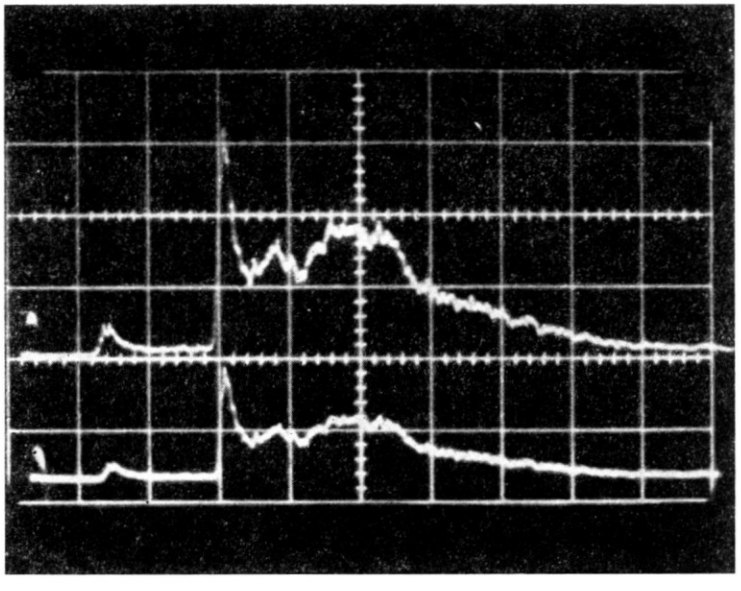

a

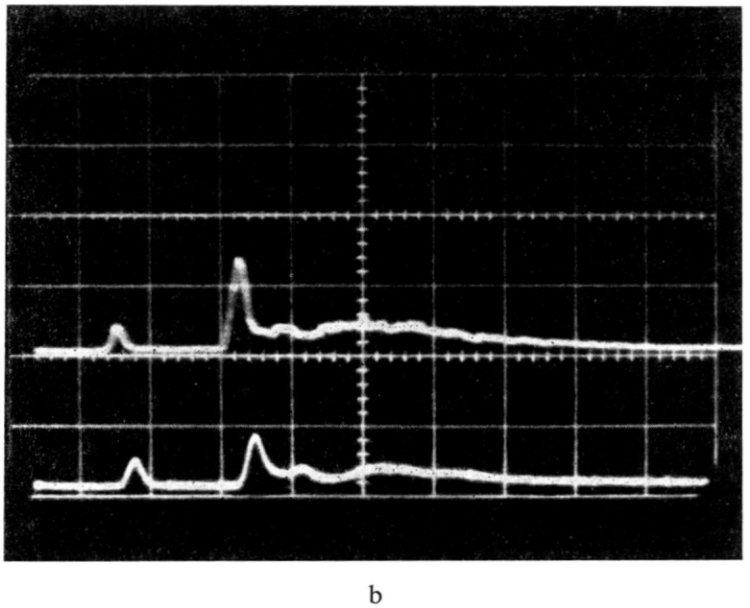

b

FIG. 10. Typical photomultiplier records. Velocity: 11400 ft/sec. Pressure: 76 mm. Sweep speed: 5 μsec/div.

(a) 1P21 result. Gain: lower beam 2 V/div. Upper beam 1 V/div.

(b) 1P28 result. Upper trace is with narrow band filter, lower trace is with wide band filter. Signal on the left is from the sphere.

In all the tests at 76 mm the trail behind the sabot showed much the same characteristics as in Fig. 10, and in a few cases, a small temporary increase in radiation could also be observed in the trail behind the sphere. At 1.65 mm pressure the radiation decreased fairly uniformly behind the sphere, however, the sabot trails showed the same characteristics as at 76 mm with the increase in radiation immediately behind the sabot being less marked. In general this "pulse" of radiation behind the body was found to be more pronounced in the ultra-violet region of the spectrum (1P28) than in the visible region (1P21 and 6217). Figure 10 shows that the fluctuations in the trail behind the sabot exist for 2–3 body diameters. This suggests that they are caused by the reverse flow field and recompression shocks behind the body. Theoretically, such flow effects should be less obvious at 1.65 mm than at 76 mm and less

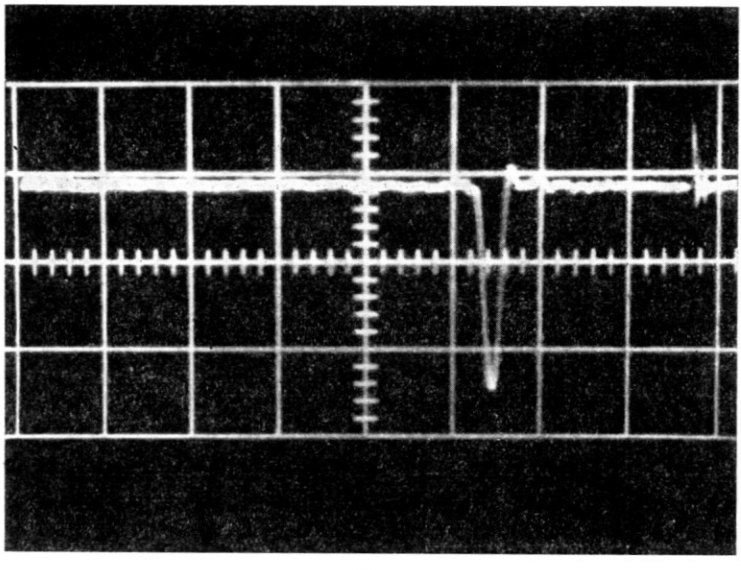

a

FIG. 11. Typical transverse microwave records. (35 Kmc/sec.)
(a) Linear polyethylene cylinder. Velocity: 14900 ft/sec. Pressure: 8 mm. Sweep speed: 100 μsec/div.

obvious behind a sphere than behind a cylinder. The experimental results are consistent with these theoretical predictions. The analysis in reference 15 was made to obtain order of magnitude estimates of trail characteristics, and for this reason does not take into account recompression shocks behind the body. The present trail results show that these effects are important and warrant inclusion in any analysis.

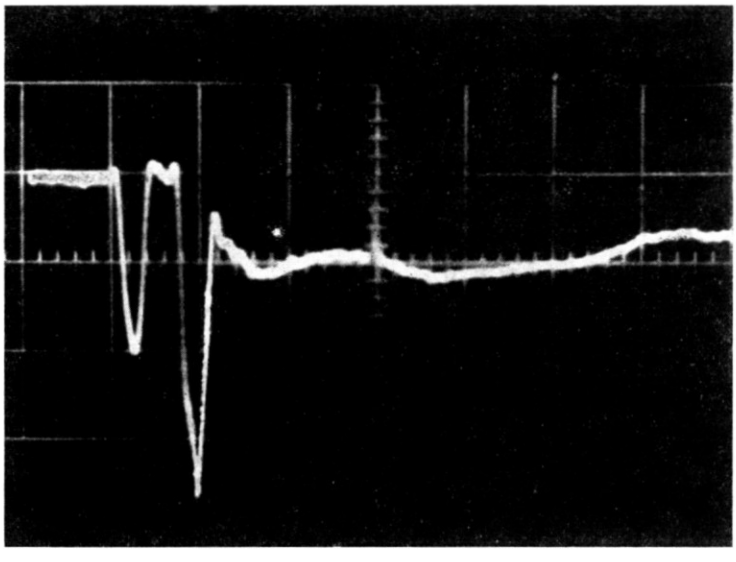

(b)

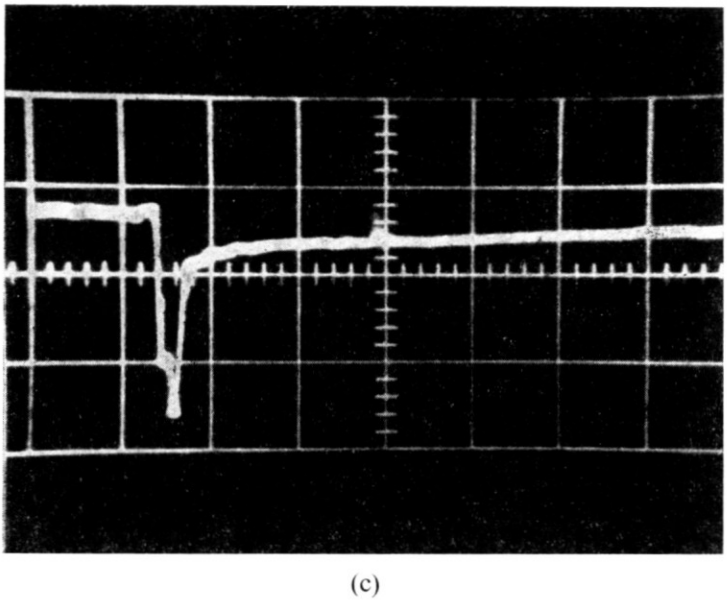

(c)

FIG. 11. Typical transverse microwave records. (35 Kmc/sec.)

(b) Ethocel sphere and linear polyethylene sabot. Velocity: 14,700 ft/sec. Pressure 8 mm. Sweep speed 50 μsec/div.

(c) Linear polyethylene cylinder. Velocity: 16,200 ft/sec. Pressure: 8 mm. Sweep speed: 50 μsec/div.

The microwave measurements were made using the 35Kmc/sec transverse unit shown in Fig. 1. The beam was focused to have a 2 in. resolution at the centre of the range and the transmitted wave was monitored. It is well known that if the frequency of an electromagnetic wave, interacting with a plasma, is less than the plasma frequency, then the wave will be cut off and no transmission will occur. Hence, in the present case, if at any point in the wake the electron density is equal to or greater than $1.5 \times 10^{13}/\text{cm}^3$ (the electron density corresponding to a plasma frequency of 35Kmc/sec), then attenuation of the beam will result. In addition to tests using spheres and sabots at 76 and 1.65 mm, several tests were conducted at other pressures using sphere/sabot combinations and cylindrical ethocel or linear polyethylene projectiles. Some typical oscilloscope traces representing transmitted signals are presented in Fig. 11. The signal is symmetrical in Fig. 11(a) and is entirely due to interruption of the beam by the projectile. Figure 11(b) corresponds to a sphere/sabot combination with no trail evident from the sphere but with a significant trail from the sabot. The other trace in Fig. 11 shows a trail behind a plastic cylinder. From such results it was possible to determine, for a given projectile and pressure, the velocity at which trails were first observed. The results are presented in Fig. 12 along with contours of constant stagnation point (electron density and plasma frequency). An arrow to the left of a point means that the trail starts at some velocity lower than that indicated. Conversely, an arrow to the right means that no trail was observed up to this velocity. Table

TABLE 2

Approximate Maximum Trail Lengths At 35 Kmc/sec

Pressure mm	Projectile	Transition vel. ft/sec	Greatest test vel. ft/sec	Trail length (body dia.)
0.15	Ethocel cyl.	> 16,500	16,500	0
1.65	Ethocel sphere	17,500	17,500	< 5
	Etchocel cyl.	16,700	17,100	< 5
	Ethocel sabot	13,200	13,200	0
	Lin. Poly. cyl.	15,500	21,600	> 130
	Lin. Poly. sabot.	14,200	17,500	> 105
8	Ethocel sphere	16,000	17,500	< 5
	Lin. Poly. cyl.	14,900	18,300	> 150
	Lin. Poly sabot.	13,000	17,500	> 150
76	Ethocel sphere	13,500	13,900	> 30
	Lin. Poly. sabot	10,400	18,600	> 350
100	Ethocel sphere	<12,800	12,800	> 60

2 has been prepared to give an indication of trail lengths observed at the greatest test velocities. The trail lengths tabulated are very approximate and are only for comparison purposes. They represent the trail length for the signal amplitude to fall to less than about 3% of the peak signal. In some cases the trails were of such length that this point has

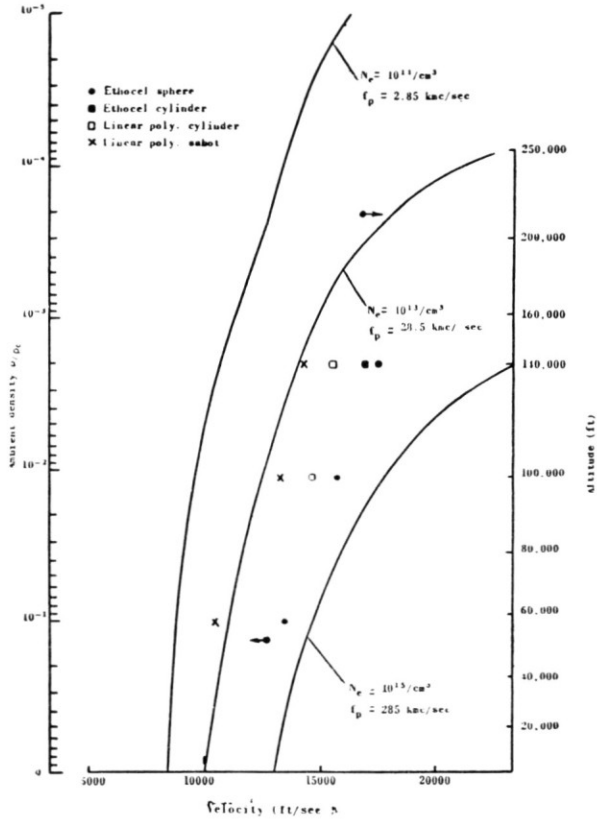

FIG. 12. Velocities at which trails appear behind various projectiles at 35 Kmc/sec.

not been reached with the available sweep time. Such cases are signified by a greater than sign in Table 2. Also, at 76 mm several results were obtained in which the trail was indicated by a positive signal as compared to negative signals shown in Fig. 11. This was attributed to a combination of the wake not being in the centre of the beam and non-uniformities in the plasma. Several points of interest arise from the results obtained. For instance there is a definite shape and material effect for a given pressure and projectile material the velocities at which trails appear are in the sequence sabot, cylinder and finally sphere. This could

be due to the fact that any ablation effects would first occur in the reverse order of velocity to that presented above. With respect to the supposition, the sabots were often slightly damaged after launching and the length of trail observed was found to increase with increasing damage. In addition, the recompression shock effects will be greater behind a cylinder or sabot than behind a sphere (see Fig. 10), and this could also lead to trails being observed behind sabots or cylinders at lower velocities than behind a sphere. The tests also revealed that, at a given pressure, linear polyethylene sabots and cylinders produced trails at lower velocities than their ethocel counterparts. This again was attributed to ablation effects due to the fact that linear polyethylene projectiles suffered more damage on launching than ethocel projectiles. Incidentally, shadowgraphs of the ethocel spheres in flight revealed no damage or distortion. The results presented in Fig. 12 represent conclusions drawn from 79 tests conducted over a six month period. The consistency of the transition points during this period was remarkable. Finally, the theoretical electron density curves from Feldman[15] indicate that at 8 mm a velocity of 19,000 ft/sec. is required before any trail effects should be observed by 35Kmc/sec. radar. Figure 12 shows that at 8 mm there is some indication of a trail developing at 16,000 ft/sec. Thus, there is reasonable agreement between experiment and theory even though theory does not take into account turbulent effects, recompression shocks behind the body and non-equilibrium effects.

4.0 CONCLUSIONS

The present paper has described some of the aerophysical studies that have been conducted in the CARDE Hypersonic Range One Facility. Due to space restrictions full details of these studies has not been given here, however, more complete information is available in references 21 22 and 23. The results obtained to date have shown that optical measurements and microwave interaction techniques are most valuable in studying the plasma surrounding a hypersonic body. Similar experimental techniques are planned for future investigations at CARDE.

ACKNOWLEDGMENTS

The results presented in this paper represent the work of many people. The radiation measurements have been the responsibility of Dr. C. St. Pierre; the microwave research has been a joint programme with Dr. R. Primich of the Defence Research Telecommunications Establishment, Ottawa; and the theoretical computations have been made with the help

of Mr. W. H. Friend. The assistance of these individuals and other members of the Hypersonic Physics Section is gratefully acknowledged. Finally, thanks are due to Dr. G. V. Bull, superintendent of the CARDE Aerophysics Wing, for his constant encouragement and advice during the course of this investigation.

REFERENCES

1. BULL, G. V., Re-entry Studies in Free Flight Ranges IAS preprint No. 59–143, 1959.
2. MAIDEN, C. J., The CARDE Hypersonic Range One Facility and Associated Research Instrumentation. CARDE TM AB-49, 1969.
3. BIOLETTI, C. and CUNNINGHAM, B. E., High Velocity Gun Employing a Shock Compressed Light Gas. NASA TN D-307, 1960.
4. RHINEHART, J. S., ALLEN, W. A. and WHITE, W. C., Phenomena Associated with the Flight of Ultra-Speed Pellets. Part II *J. App. Phys.*, **23**, No. 2, 198, 1952.
5. ALLEN, W. A. and MAYFIELD, E. B., Time-resolved Spectroscopy of Ultra-Speed Pellet Luminosity. *J. App. Phys.* **24**, No. 2, 131, 1953.
6. DAVIDSON, R. A. and PARTRIDGE, W. S., Time lag between High-Speed Pellets and the Ionisation in Their Trails. *J. App. Phys.* **28**, No. 11, 1957.
7. SHKAROFSKY, I. P., JOHNSTON, T. W. and BACHYNSKI, M. P., Relaxation Phenomena in Shock Fronts. Proc. of Symposium on the Plasma Sheath, **1**, AFCRC-TR-60–108, 1959.
8. FELDMAN, S., Hypersonic Gas Dynamic Charts for Equilibrium Air. AVCO Res. Lab. Research Note No. 25, 1957.
9. GILMORE, F. R., Equilibrium Composition and Thermodynamic Properties of Air to 24,000°K. Rand RM-1543, 1955.
10. MASLEN, S. H. and MOECKEL, W. E., Inviscid Hypersonic Flow Past Blunt Bodies. *J. Aero. Sci.* **24**, 683, 1957.
11. HAYES, W. D. and PROBSTEIN, R. F., *Hypersonic Flow Theory*. Academic Press., 1959.
12. HOCKSTIM, A. R., Air in Equilibrium for Normal Shocks at Hypersonic Velocities. Convair Report No. Zph. 002, 1957.
13. KECK, J. C., KIVEL, B. and WENTINK, T., Emissivity of High Temperature Air. AVCO Res. Lab. Research Note No. 8, 1957.
14. International Critical Tables, Vol. V, p. 238.
15. FELDMAN, S., Trails of Axi-Symmetric Hypersonic Blunt Bodies Flying Through the Atmosphere. AVCO Res. Lab. Research. Rept. No. 82, 1959.
16. HAMMERLING, P., TEARE, J. D. and KIVEL, B., Radiation From Nitrogen Shock Fronts. *Pull. Am. Phys. Soc., Series* II, **4**, 1959 No. 1.
17. CAMM, J. C. and KECK, J. C., Spectrographic Studies of Shock Fronts in Nitrogen. *Bull. Am. Phys. Soc., Series* II, **4**, 1959.
18. ST. PIERRE, C. A., The Visible Emission from 1/2″ Hypervelocity Models measured with a Moving Target Scan Monochromator. CARDE TM AB-59, 1960.
19. KECK, J. C., CAMM, J. C., KIVEL, B. and WENTINK, T., Radiation from Hot Air. Part II. Shock Tube Study of Absolute Intensities. *Ann. Phys.* **7**, 1959.

20. GOULARD, R., The Aerothermodynamics of Re-entry Trails. Am. Rocket Soc. preprint No. 1145–60, 1960.

21. ST. PIERRE, C. A., Emitted Radiation Studies Performed in a Hypersonic Range with Half-inch Models. CARDE TM AB-52, 1960.

22. MAIDEN, C. J. and ST. PIERRE, C. A., Some measurements of the Physical Properties of the Plasma Sheath Around Hypersonic Projectiles. CARDE TM AB-56, 1960.

23. ST. PIERRE, C. A. and MAIDEN, C. J., Results from the Second Radiation Programe in CARDE Hypersonic Range One using Half-inch Models. CARDE TM AB-61, 1960